Electron heating at Saturn's bow shock

A. Masters,[1,2] S. J. Schwartz,[3] E. M. Henley,[3] M. F. Thomsen,[4] B. Zieger,[5] A. J. Coates,[1,2] N. Achilleos,[6,7] J. Mitchell,[3] K. C. Hansen,[8] and M. K. Dougherty[3]

Received 17 June 2011; revised 3 August 2011; accepted 4 August 2011; published 28 October 2011.

[1] Collisionless shock waves are a widespread phenomenon in both solar system and astrophysical contexts. The nature of energy dissipation at such shocks is of particular interest, especially at high Mach numbers. We use data taken by the Cassini spacecraft to investigate electron heating at Saturn's bow shock, one of the strongest collisionless shocks encountered by spacecraft to date. Measurements of the upstream solar wind ion parameters are scarce due to spacecraft pointing constraints and the absence of an upstream monitor. To address this, we use solar wind speed predictions from the Michigan Solar Wind Model. Since these model predictions are based on near-Earth solar wind measurements, we restrict our analysis to bow shock crossings made by Cassini within ±75 days of apparent opposition of Earth and Saturn. An analysis of the resulting set of 94 crossings made in 2005 and 2007 reveals a positive correlation between the electron temperature increase across the shock and the kinetic energy of an incident proton, where electron heating accounts for between ~3% and ~7% of this incident ram energy. This percentage decreases with increasing Alfvén Mach number, a trend that we confirm continues into the hitherto poorly explored high–Mach number regime, up to an Alfvén Mach number of ~150. This work reveals that further studies of the Saturnian bow shock will bridge the gap between the more modest Mach numbers encountered in near-Earth space and more exotic astrophysical regimes where shock processes play central roles.

Citation: Masters, A., S. J. Schwartz, E. M. Henley, M. F. Thomsen, B. Zieger, A. J. Coates, N. Achilleos, J. Mitchell, K. C. Hansen, and M. K. Dougherty (2011), Electron heating at Saturn's bow shock, *J. Geophys. Res.*, *116*, A10107, doi:10.1029/2011JA016941.

1. Introduction

[2] A shock wave forms when the speed of a flow relative to an obstacle is faster than the speed at which information about the obstacle's presence can propagate in the surrounding fluid (e.g., via sound waves in the case of a collisional, neutral gas). Across the shock there is an abrupt change in the flow properties, where, in general, the flow speed decreases and the temperature and density of the fluid increases. The shock processing of the fluid from upstream to downstream allows it to flow around the obstacle.

[3] The discovery of shock waves in space plasmas was surprising to many researchers because of the effective absence of collisions in these tenuous media [*Fairfield*, 1976, and references therein]. In such collisionless plasmas the collisional interaction between particles is replaced by an interaction via electromagnetic fields. A cross-shock potential difference couples the electron and ion fluids [e.g., *Formisano*, 1982], while influencing the kinetic dynamics in ways that disperse particle trajectories and hence convert directed into random motion. Collisionless shocks in space are frequently observed by spacecraft since they stand upstream of planetary obstacles to the solar wind (planetary bow shocks, see the review by *Russell* [1985]) and can also result from the interaction between different solar wind flow streams (interplanetary shocks, see the review by *Smith* [1985]).

[4] An important property of a collisionless shock is its Mach number, defined as the upstream flow speed divided by a characteristic upstream wave speed. In a space plasma the wave of interest is the fast magnetosonic wave (which steepens to form the shock), characterized by the fast magnetosonic Mach number M_f (always >1 for shocks, by definition). The critical Mach number M_C is defined as the Mach number at which the flow speed immediately downstream

[1]Mullard Space Science Laboratory, Department of Space and Climate Physics, University College London, Surrey, UK.
[2]Also at Centre for Planetary Sciences, University College London–Birkbeck, London, UK.
[3]Space and Atmospheric Physics Group, Blackett Laboratory, Imperial College London, London, UK.
[4]Space Science and Applications, Los Alamos National Laboratory, Los Alamos, New Mexico, USA.
[5]Space Research Institute, Austrian Academy of Sciences, Graz, Austria.
[6]Centre for Planetary Sciences, University College London–Birkbeck, London, UK.
[7]Atmospheric Physics Laboratory, Department of Physics and Astronomy, University College London, London, UK.
[8]Department of Atmospheric, Oceanic, and Space Sciences, University of Michigan, Ann Arbor, Michigan, USA.

0148-0227/11/2011JA016941

of the shock is equal to the local sound speed [*Kennel et al.*, 1985]. The nature of energy dissipation at the shock depends on whether the shock is subcritical ($M_f < M_C$) or supercritical ($M_f > M_C$). The speed of upstream Alfvén waves is often also used to define an Alfvén Mach number M_A. Another important parameter is the shock angle θ_{Bn}, defined as the angle between the upstream magnetic field and the normal to the shock surface (between 0° and 90°), which plays an important role in controlling shock structure. When studying a collisionless shock a popular reference frame is the deHoffmann-Teller (H-T) frame, which is defined such that the motional electric field has a magnitude of 0 both upstream and downstream.

[5] Earth's bow shock forms due to the obstacle presented to the solar wind flow by the planet's intrinsic magnetic field, producing a cavity in the flow known as a magnetosphere. Given its proximity to Earth relative to other collisionless shocks in the solar system, the terrestrial bow shock is understandably one of the most frequently observed by spacecraft, and much of our understanding of these waves is based on in situ spacecraft observations of this shock.

[6] M_f values for Earth's bow shock range between ~3 and ~10 [e.g., *Peredo et al.*, 1995]. θ_{Bn} varies across the shock surface, and is strongly controlled by the orientation of the upstream Interplanetary Magnetic Field (IMF). For θ_{Bn} values less then 45° the shock is referred to as quasi-parallel, where particles move back upstream along magnetic field lines, producing an extended upstream-downstream transition (see the review by *Burgess et al.* [2005]). However, when θ_{Bn} is greater than 45° the shock is referred to as quasi-perpendicular, and particles that escape back upstream are largely confined to gyrate about magnetic field lines in front of the shock, producing a more abrupt upstream-downstream transition [*Woods*, 1971] (see the review by *Bale et al.* [2005]). When supercritical, ion reflection by the cross-shock potential leads to efficient ion energization from upstream to downstream essential for the dissipation of bulk flow energy [*Sckopke et al.*, 1983] (see the reviews by *Gosling and Robson* [1985] and *Gedalin* [1997]).

[7] Compared to the heating of ions, electron heating at collisionless shocks is generally small, which was a surprising result when it was first measured for Earth's bow shock [*Thomsen et al.*, 1987, and references therein]. Current understanding is that shock electron heating is due to the phase space inflation of the electron distribution in the presence of the cross-shock potential in the H-T frame [*Feldman et al.*, 1982; *Goodrich and Scudder*, 1984] (see the review by *Scudder* [1995]). *Thomsen et al.* [1987] analyzed 52 crossings of Earth's bow shock and found that the electron temperature difference across the shock was best correlated with the change in bulk flow energy, showing a positive correlation. This result is in agreement with electron heating being dominated by the macroscopic cross-shock potential. *Schwartz et al.* [1988] examined shock electron heating further using observations of various collisionless shocks in the solar system and showed that the fraction of the dissipated energy that is transferred into electron thermal energy also decreases as the shock Mach number (M_f or M_A) increases. The reason for this Mach number dependence remains unclear; however, possible explanations include greater anomalous resistive heating at lower Mach numbers [*Schwartz et al.*, 1988]. Further work on electron heating at Earth's bow shock based on spacecraft observations carried out by *Hull et al.* [2000] supports the earlier findings of both *Thomsen et al.* [1987] and *Schwartz et al.* [1988].

[8] Since Saturn is a magnetized gas giant planet it has a large magnetosphere and an associated bow shock. Owing to the different solar wind conditions at Earth and Saturn the Mach numbers associated with Saturn's bow shock are higher than those at Earth [*Slavin et al.*, 1985], and indeed is one of the strongest shocks ever encountered by spacecraft. The Cassini spacecraft has been orbiting Saturn since July 2004 and has crossed the planetary bow shock on hundreds of occasions, providing an opportunity to examine a shock wave that could shed light on the processes operating at high–Mach number astrophysical shocks.

[9] Data taken during Cassini's first planetary orbit was used by *Achilleos et al.* [2006] to determine the typical properties of Saturn's bow shock. Most of the crossings studied by these authors were encounters with the shock under quasi-perpendicular conditions, and always supercritical ($M_f \sim 15$). They inferred that the shock ramp thickness was of order 1 proton inertial length, consistent with the anticipated importance of ion kinetics for energy dissipation, and estimated the speed of the shock front in the planet's rest frame to be of order 100 km s^{-1}.

[10] In this paper we use Cassini observations made during crossings of Saturn's bow shock to investigate electron heating at the shock. We show that the electron temperature difference across the shock increases as the incident proton kinetic energy increases, in agreement with our current understanding of electron heating at collisionless shocks. The electron heating accounts for between ~3% and ~7% of the incident proton kinetic energy, and this percentage decreases with increasing M_A. The highest values of M_A in our set of crossings are among the highest that have ever been reported based on in situ spacecraft observations.

2. Determining Upstream and Downstream Parameters

2.1. Cassini Observations

[11] The coordinate system used throughout this study is the kronocentric solar magnetospheric (KSM) system, which is Saturn centered, with the positive x axis pointing toward the Sun. The z axis is chosen such that the xz plane contains Saturn's magnetic dipole axis, with the positive z axis pointing in the same sense as Saturn's North Pole. The y axis completes the orthogonal set, with the positive y axis pointing toward dusk.

[12] The fluxgate magnetometer sensor of the Cassini dual-technique magnetometer [*Dougherty et al.*, 2004] provides measurements of the magnetic field, and the electron spectrometer sensor (ELS) of the Cassini plasma spectrometer detects electrons between 0.6 eV and 27 keV [*Young et al.*, 2004]. Cassini is a three-axis stabilized spacecraft, which introduces pointing constraints on the measurement of the thermal ion population in environments that include the near–bow shock solar wind, since the ion thermal speed is typically far less than the bulk flow speed [e.g., *Thomsen et al.*, 2010]. This pointing issue does not apply to electrons in the vicinity of the shock as they have a thermal speed that is typically far higher than the bulk flow speed, meaning that ELS is able to detect the ambient

electron distribution regardless of the instrument pointing direction [e.g., *Lewis et al.*, 2008]. Where appropriate, electron moments are derived from background-subtracted data taken by ELS anode 5, based on the assumption of an isotropic distribution in the spacecraft frame [*Lewis et al.*, 2008]. The detailed analysis of any specific shock crossings where ion data may be available is worthy of future study.

[13] Figure 1 shows magnetic field and electron data taken by Cassini during two crossings of Saturn's bow shock. Crossing 1 (Figures 1a–1c) has been chosen as it is typical of the observed shock signatures, whereas crossing 2 (Figures 1d–1f) has been chosen because it has an atypical signature. In crossing 1 the spacecraft began the interval upstream of the shock and ended the interval downstream of the shock (an inbound crossing). There was a steep increase in the field strength at the shock (known as the shock "ramp") followed by an overshoot and undershoot in the field strength characteristic of a supercritical, quasi-perpendicular shock [e.g., *Russell et al.*, 1982]. Electrons were detected upstream of the shock predominantly below ~10 eV, with two components evident in this case. The higher-energy component is the ambient solar wind electron population, and the second, lower-energy component corresponds to photoelectrons that originate from the surfaces of the sunlit spacecraft, driving the spacecraft potential a few volts positive. Downstream of the shock the heated ambient electron population was detected between energies of ~30 and ~400 eV, and spacecraft photoelectrons were detected below ~5 eV. The superposition of electron populations in the upstream region poses significant difficulties for the derivation of reliable electron moments [*Masters et al.*, 2008, 2009], whereas the near-isotropic downstream distribution is much more distinct, and leads to reliable electron number densities and temperatures.

[14] Crossing 2 has a very different signature. The spacecraft began the interval downstream of the shock and ended the interval upstream of the shock (an outbound crossing). The magnetic signature was very disturbed, without the single, localized change in magnetic field strength observed at crossing 1. The series of field strength enhancements detected between ~0115 and ~0125 UT may have been multiple encounters with the shock, or examples of upstream phenomena (see the review by *Eastwood et al.* [2005]). The electron signature is broadly similar to that of crossing 1; however the downstream electron moments reveal a far denser and colder electron environment, which produces a highly unusual spacecraft potential for this environment of ~0 V. We note that these two crossings (and the others included in our data set) resulted from motion of the shock away from/toward the planet for inbound/outbound crossings, respectively. This results from a small spacecraft speed (a few kilometers per second) compared to the shock speed (order 100 km s^{-1}) in the rest frame of the planet [*Achilleos et al.*, 2006].

[15] The data presented in Figure 1 illustrate what properties can be derived from Cassini data both upstream and downstream of the shock. Although the magnetic environment is well defined in both regimes, as are the electron number densities and temperatures downstream, upstream electron number densities and temperatures are not reliable due to the presence of spacecraft photoelectrons. However, we can place limits on the upstream electron temperature by constraining it to be greater than 0 eV and less than the approximate energy at which electron differential energy flux abruptly decreases (~10 eV in the case of crossing 1). In some cases (e.g., crossing 1) it may be possible to constrain the upstream electron temperature more accurately than by using this conservative approach; however, the difference in the electron temperature across the shock is dominated by the downstream temperature, and the conclusions that we draw based on the electron heating results presented in section 4 would not be affected by reducing the uncertainties associated with the electron temperature difference by addressing the upstream electron temperatures further.

[16] A particularly important upstream parameter is the bulk flow velocity, measurements of which are unavailable due to the general inability of the Cassini ion spectrometer to view the solar direction and the absence of a dedicated upstream monitor. To address this we used upstream flow speed predictions made by a simulation of the solar wind that uses spacecraft observations as boundary conditions.

2.2. Solar Wind Model and Selected Crossings

[17] The Michigan Solar Wind Model (MSWiM) is a one-dimensional (1-D) magnetohydrodynamic code that propagates solar wind parameters from 1 Astronomical unit (AU) to Saturn's orbital distance of ~10 AU [*Zieger and Hansen*, 2008]. Solar wind conditions at 1 AU are measured by near-Earth spacecraft and provide boundary conditions for the model, which simulates the evolution of these properties as heliocentric distance increases. These predictions are hereafter referred to as "propagations."

[18] The validity of MSWiM propagations was discussed in detail by *Zieger and Hansen* [2008]. They compared the model propagations to observations made by a number of spacecraft that have explored the heliosphere (e.g., Voyager). They found that the accuracy of the propagations was higher the closer the time of interest was to a time of apparent opposition between Earth and the target object (e.g., Saturn). Opposition is defined as Sun-Earth-target alignment (in that order), whereas apparent opposition takes into account the transit time of the solar wind between Earth and the target object. In addition they found that the propagation accuracy was higher during times when the solar wind speed followed a recurring pattern, which is typical of the declining phase of the solar cycle when the solar corona is relatively stable. The propagated solar wind parameter that showed the best agreement with spacecraft observations was the solar wind speed. *Zieger and Hansen* [2008] also determined the error in the time of arrival of a propagated region of solar wind (~20 h at apparent opposition during the declining phase, compared to typical propagation times from 1 AU to Saturn of 30 days), which allows us to assign an uncertainty to the model predictions by considering all the propagations within the error window of a time of interest.

[19] Fortunately the early phase of Cassini's orbital tour of Saturn (2004–2007) corresponded to the desirable declining phase of the solar cycle, when the solar wind observed at Saturn's orbit exhibited a repeating pattern of compressions and rarefactions associated with corotating interaction regions [*Jackman et al.*, 2004]. In this study we use MSWiM solar wind propagations to provide a measure of the flow speed upstream of Saturn's bow shock. We assumed that the solar wind velocity vector pointed radially away from the Sun.

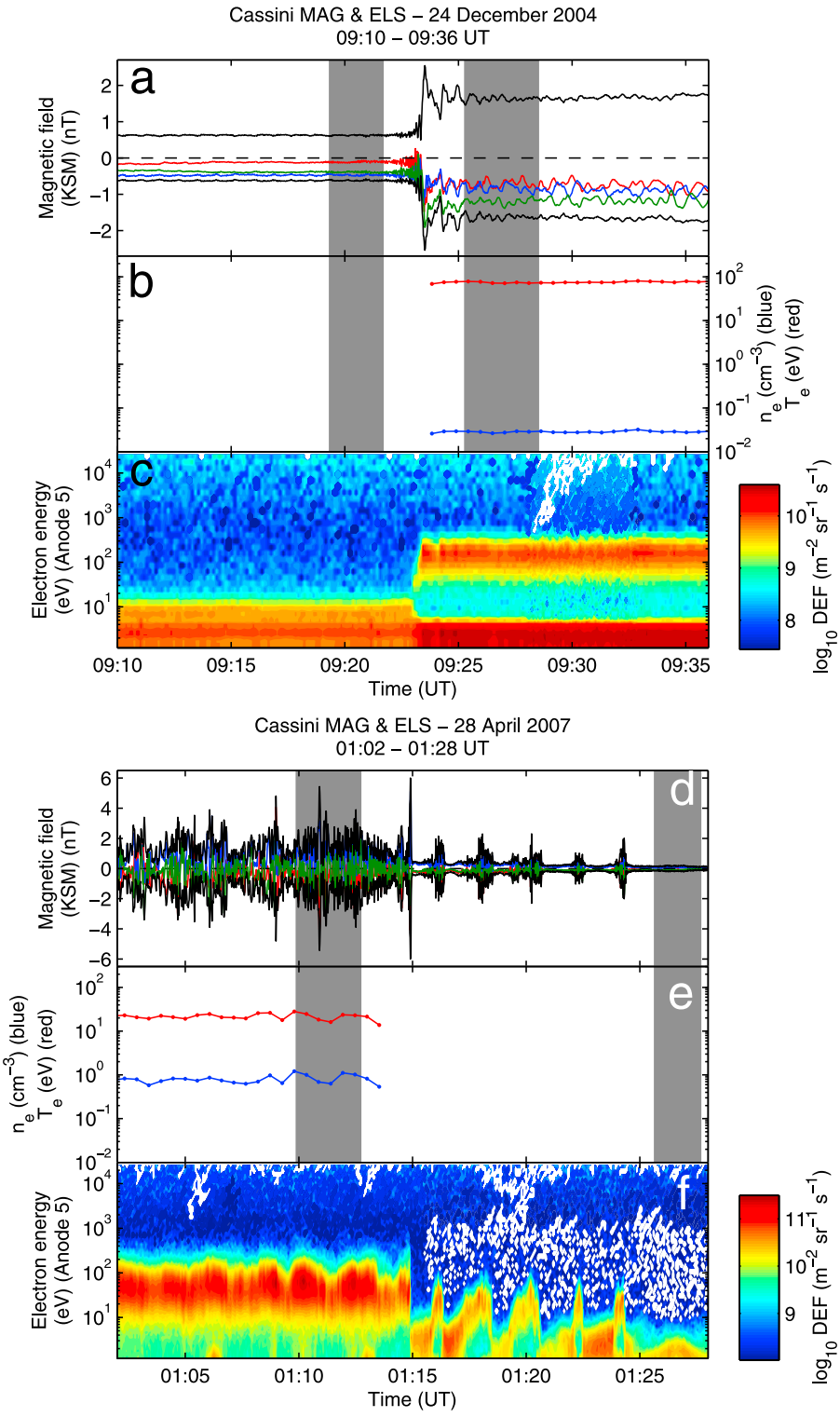

Figure 1. Cassini observations made during bow shock crossings on (top) 24 December 2004 and on (bottom) 28 April 2007. (a, d) Magnetic field in kronocentric solar magnetospheric (KSM) coordinates. Black, red, blue, and green are the field strength, x component, y component, and z component, respectively. (b, e) Electron number density and temperature derived from ELS anode 5. (c, f) Energy-time spectrogram of electron differential energy flux (DEF) from ELS anode 5. Shaded intervals indicate chosen upstream and downstream intervals. Shock properties for the 24 December 2004 crossing are $\theta_{Bn} \sim 65°$, $M_A^* = 3 \pm 1$. Shock properties for the 28 April 2007 crossing are $\theta_{Bn} \sim 55°$, $M_A^* = 40 \pm 20$. See section 3 for a description of how these shock properties were determined.

Between the beginning of 2004 and the end of 2007 there were three times of apparent opposition between Earth and Saturn. Since *Zieger and Hansen* [2008] showed that the accuracy of the speed propagations is relatively constant within approximately ±75 days of apparent opposition we limited our analysis to bow shock crossings made by Cassini within these ±75 day intervals.

[20] Owing to the spacecraft trajectory, Cassini only made bow shock crossings in 2005 and 2007 that were within ±75 days of a time of apparent opposition. Figure 2 shows the positions of this set of 94 crossings that are the focus of this study. The 2005 crossings took place at low latitudes on the dawn side of the shock, and the 2007 crossings took place on the dusk side at higher latitudes. The large spread in the positions of these crossings is due to the highly variable position of the bow shock [*Went et al.*, 2011], due to the similarly high level of variability in the size of the magnetospheric obstacle [*Kanani et al.*, 2010].

[21] Upstream and downstream properties were extracted from the magnetic field and electron data for each of these crossings (see section 2.1) by choosing an interval of a few minutes on each side of the shock where the measured conditions were steady. The downstream electron environment was generally stable (see Figure 1), making our analysis insensitive to the exact choice of downstream interval at each crossing. The upstream interval was chosen to capture the unperturbed upstream field, and may not reflect the upstream field vector at the exact time of a shock crossing (see Figure 1d); however, since the majority of the shock crossing signatures resemble the example of crossing 1 (see Figure 1a) we concluded that our upstream interval definition was appropriate for this analysis. The approximate time of a shock crossing was used to define an error window [*Zieger and Hansen*, 2008] within which all the propagated solar wind speeds from MSWiM were extracted. The propagated speed value closest to the shock crossing time was taken as the solar wind speed, and the range of values in the error window was taken as the uncertainty in this speed.

[22] In sections 3 and 4 we use this set of 94 crossings with their associated upstream and downstream parameters (both measured in situ and propagated) to determine the typical properties of Saturn's bow shock, and to assess the nature of electron heating at the shock.

3. Shock Properties

[23] Using the plasma parameters upstream and downstream of the shock discussed in section 2 we were able to calculate a number of shock properties for each Cassini crossing. These properties are presented in Figure 3, and their derivation is outlined in this section.

[24] The value of θ_{Bn} for each crossing was determined using the measured upstream magnetic field and a normal vector to the local bow shock surface given by the prediction of the global shock surface model constructed by *Went et al.* [2011]. We favor the use of such model normals throughout our analysis because studies of Earth's bow shock suggest that model normals are most appropriate for single-spacecraft shock studies [*Horbury et al.*, 2002]. Shock normals given by the alternative methods of coplanarity analysis and minimum variance analysis are generally unreliable due to the high level of variability of the downstream magnetic field and the poor definition of the field variance directions, respectively. Figure 3a shows a histogram of the calculated values of θ_{Bn}. The majority of the shock crossings were quasi-perpendicular, most likely due to the prevailing IMF conditions at Saturn [*Jackman et al.*, 2008].

[25] Further information about the upstream medium is required in order to calculate any of the shock Mach numbers. In this study we only consider M_A as its calculation only requires the inference of one additional upstream parameter: The upstream plasma mass density ρ_u. M_A is defined as

$$M_A = \frac{v_u(\mu_0\rho_u)^{\frac{1}{2}}}{B_u}, \tag{1}$$

where v_u is the upstream flow speed normal to the shock, μ_0 is the permeability of free space, and B_u is the upstream magnetic field strength. As discussed in section 2, the upstream plasma density is not provided by in situ Cassini observations. In addition, MSWiM density propagations are not as reliable as the speed propagations [*Zieger and Hansen*, 2008], and these density propagations are often associated with uncertainties of order 100%.

[26] To infer the upstream mass density we assumed that the shock was exactly perpendicular at each crossing (θ_{Bn} = 90°). This assumption was motivated by the fact that for perpendicular shocks the shock compression ratio r can be expressed as

$$r = \frac{\rho_d}{\rho_u} = \frac{B_d}{B_u}, \tag{2}$$

where ρ_d is the downstream mass density and B_d is the downstream magnetic field strength [e.g., *Burgess*, 1995]. This assumption allows us to infer the upstream mass density using the measured ratio of magnetic field strengths and the measured downstream electron number density, assuming that the plasma is charge neutral. Although the values of θ_{Bn} presented in Figure 3a suggests that assuming a perpendicular shock is reasonable, this assumption will be inappropriate for some of the crossings. Figure 3b shows a histogram of the measured magnetic field strength ratios. Outlying data points likely correspond to cases where the perpendicular shock assumption is particularly invalid. However, the median of these ratios is 4.4, consistent with the widely used value of the shock compression ratio for high–Mach number shocks of 4 [e.g., *Burgess*, 1995]. As a result, we assume a shock compression ratio of 4 ± 1 for all the shock crossings considered in this study (this uncertainty is based on the lower and upper quartiles of the distribution shown in Figure 3b: 3.2 and 5.4). This allows us to infer the upstream number density at each crossing, all of which have smaller uncertainties than the MSWiM density propagations but agree with the MSWiM densities to within the uncertainties.

[27] The speed of the shock surface is also relevant for M_A calculations. As discussed in section 2.2, Saturn's bow shock moves at a much greater speed than that of Cassini relative to Saturn. To estimate the speed of the shock we use the same approach that was outlined by *Gosling and Thomsen* [1985] and employed by *Achilleos et al.* [2006].

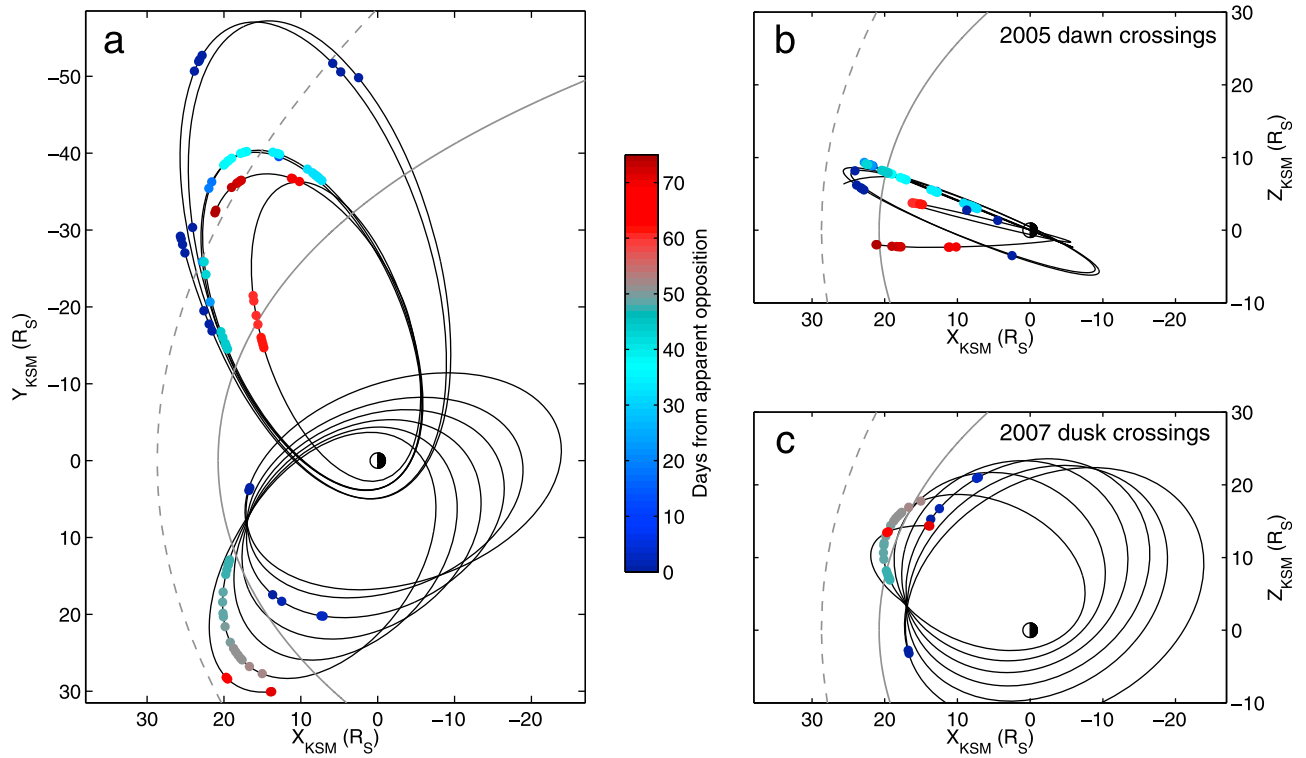

Figure 2. Bow shock crossings that took place within ±75 days of a time of apparent opposition in 2005 and 2007. (a) Bow shock crossings (colored dots) and associated spacecraft trajectory (curves) projected onto the *xy* plane of the KSM system. (b) Bow shock crossings (colored dots) and associated spacecraft trajectory (curves) for the 2005 crossings only, projected onto the *xz* plane of the KSM system. (c) Bow shock crossings (colored dots) and associated spacecraft trajectory (curves) for the 2007 crossings only, projected onto the *xz* plane of the KSM system. The color bar indicates how close to a time of apparent opposition each crossing took place. The solid and dashed shaded curves indicate the intersection of the typical positions of Saturn's magnetopause (the boundary of the magnetosphere) and bow shock with each plane, respectively [*Kanani et al.*, 2010; *Went et al.*, 2011].

The turnaround distance of an incident proton that is specularly reflected at a 1-D shock d is given by

$$d = \left(\frac{v_u}{\Omega_u}\right)\left(\psi\left(2\cos^2\theta_{Bn} - 1\right) + 2\sin^2\theta_{Bn}\sin\psi\right), \qquad (3)$$

where Ω_u is the upstream proton gyrofrequency, and ψ is given as

$$\cos\psi = \frac{1 - 2\cos^2\theta_{Bn}}{2\sin^2\theta_{Bn}}. \qquad (4)$$

This distance can only be evaluated for $\theta_{Bn} > 30$. This region of gyrating ions immediately in front of the shock ramp is known as the shock "foot," as it produces a region in front of the ramp where the field is elevated above the upstream level (see the review by *Bale et al.* [2005]). We note that at shocks with $\theta_{Bn} < 39.9°$ a specularly reflected ion moves upstream and never returns to the shock, thus encounters with the shock under such quasi-parallel conditions are unlikely to have a clear foot feature [*Schwartz et al.*, 1983]. By measuring the duration of the shock foot at each crossing, using equation (3) to calculate the spatial scale of the shock foot, and taking into account the spacecraft motion (a relatively minor effect), we can estimate the shock speed.

[28] Figure 4 shows the magnetic field strength measured during the same Cassini bow shock crossing that is also shown in Figure 1a. The ramp is clear, and a linear fit to this feature is shown as the slanted dashed line. The mean upstream field strength is shown as a horizontal dashed line. The shock foot feature was present in this case. We define the shock foot interval as the time between the time of intersection of the two dashed lines, and the time at which the upstream field strength rose above a threshold value of four standard deviations above the mean field strength in the upstream interval. The foot interval is shown as a shaded interval in Figure 4. Like *Achilleos et al.* [2006], we treat these values as order of magnitude estimates of the shock speed. Furthermore, the shock foot was ambiguous at 42 crossings, excluding them from this part of our analysis.

[29] Figure 3c shows a histogram of the shock normal component of the solar wind velocity at the shock crossings (generally between 300 and 500 km s^{-1}) and Figure 3d shows a histogram of the estimated shock speeds. These shock speeds were estimated at 52 crossings, and were generally of order 100 km s^{-1} both toward and away from the planet, in agreement with the results of *Achilleos et al.* [2006]. Figure 3e shows a histogram of values of M_A that were calculated assuming the shock was stationary each time it was encountered by the spacecraft (equation (1)).

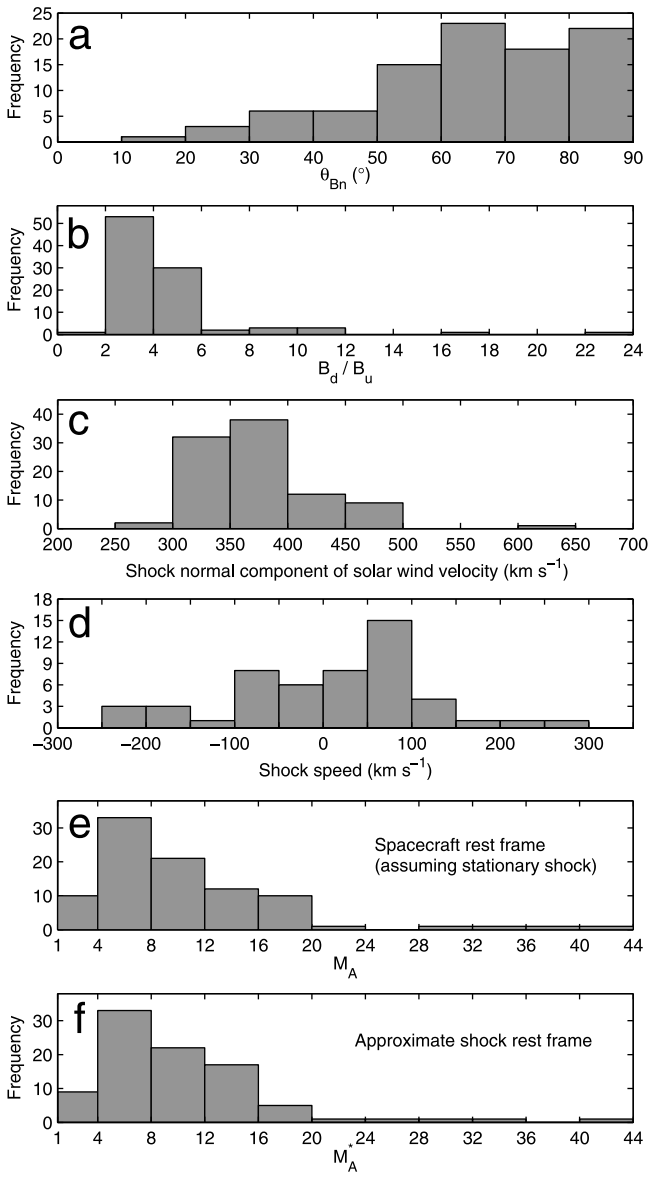

Figure 3. Properties of the included Cassini bow shock crossings. (a) Histogram of shock angles θ_{Bn}. (b) Histogram of the magnetic field strength ratio B_d/B_u. (c) Histogram of the shock normal component of the solar wind velocity. (d) Histogram of estimated shock speeds in the normal direction based on the identification of the shock foot. Positive values are away from the planet, and negative values are toward the planet. (e) Histogram of Alfvén Mach numbers based on the assumption of a stationary shock M_A. (f) Histogram of Alfvén Mach numbers based on the assumption of shock speed at +100 km s^{-1} for inbound crossings and −100 km s^{-1} for outbound crossings M_A* (where positive values are away from the planet and negative values are toward the planet).

However, in order to examine electron energetics at Saturn's bow shock the normal component of the upstream flow velocity in the shock rest frame shock is required. Figure 3f shows a histogram of M_A*, Alfvén Mach number values calculated in the approximate shock rest frame based on the assumption that the shock was moving at a speed of 100 km s^{-1} away from/toward the planet in the local normal direction for inbound/outbound crossings.

[30] The M_A values presented in the histograms in both Figures 3e and 3f are in agreement with previous measurements based on Pioneer and Voyager data [*Slavin et al.*, 1985]. Some values are above 44, and are presented in section 4. These results confirm a typically higher value of M_A for Saturn's bow shock than for Earth's bow shock [e.g., *Schwartz et al.*, 1988].

4. Electron Heating

[31] To investigate electron heating at Saturn's bow shock we defined the upstream electron temperature at each crossing to be half the identified upper limit (see section 2.1), with an associated uncertainty of 100%. This leads to values of the electron temperature difference across Saturn's bow shock ΔT_e. Figure 5 shows how ΔT_e varies with the kinetic energy associated with the normal component of the velocity of an upstream proton. In Figure 5a no correction for shock motion has been applied, corresponding to the assumption of a stationary shock for all crossings. There is a reasonable positive correlation between these two quantities, which is expected based on studies of electron heating at Earth's bow shock [e.g., *Thomsen et al.*, 1987]; however, there are a number of outlying data points.

[32] Since the shock speed is of order 100 km s^{-1} it is expected to be an important factor in controlling the normal component of the upstream flow velocity in the rest frame of the shock. In Figure 5b the colors of the data points have been chosen to differentiate between inbound and outbound crossings. At inbound crossings the shock was moving away from the planet, producing a greater normal upstream flow component than implied by the associated solar wind speed, and vice versa for outbound crossings. In Figure 5b it is clear that the electron heating was generally greater at inbound crossings than at outbound crossings, confirming that shock motion is a major effect. Furthermore, the outlying data points associated with relatively large temperature differences are all inbound crossings, and those at relatively low differences are predominantly outbound crossings.

[33] In Figures 5c and 5d a correction for shock motion has been applied. Although shock speeds based on observations of the shock foot feature only apply to 52 of the 94 crossings they are employed in Figure 5c to attempt to use the shock rest frame where possible. This correction produces a clearer positive correlation. However, the approach to correcting for shock motion that we favor is to assume a shock speed of 100 km s^{-1} away from/toward the planet in the normal direction for inbound/outbound crossings, with an associated uncertainty of 100 km s^{-1} in each case. This allows for a stationary shock and a shock moving at a maximum speed of 200 km s^{-1}, in agreement with the results presented in Figure 3d. The corrected results based on this approach are shown in Figure 5d, where the positive correlation and the inbound-outbound difference in electron heating are particularly clear.

[34] We favor the approach shown in Figure 5d over that shown in Figure 5c because it does not rely on the identification of the shock foot for each crossing, and the speed determinations based on the shock foot should only

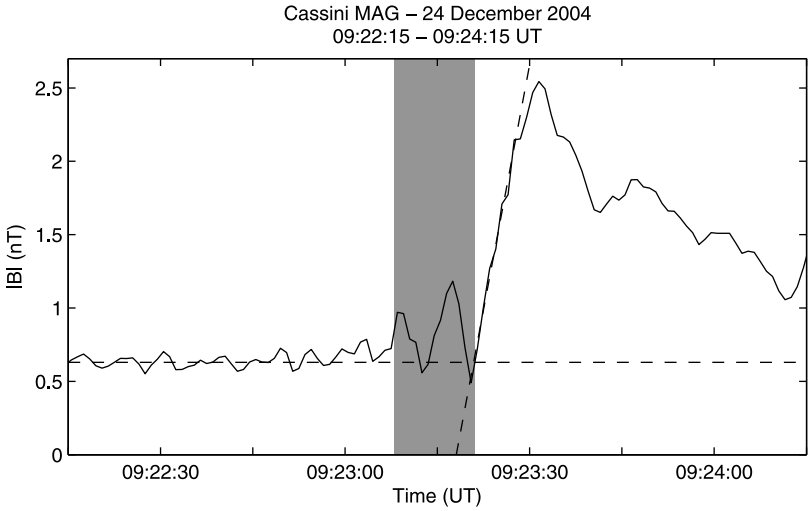

Figure 4. Cassini measurements of the magnetic field strength during a bow shock crossing on 24 December 2004. Dashed lines indicate the mean upstream field strength (horizontal) and a linear fit to the shock ramp (slanted) that are used to define the duration of the shock foot. The shock foot interval is shaded.

be treated as order of magnitude estimates [e.g., *Achilleos et al.*, 2006]. However, our chosen approach is not perfect, and results in the separation of the data set into two subsets (inbound and outboung crossings) that do not overlap in incident ion kinetic energy despite overlapping significantly in electron temperature difference (see Figure 5d). But, nonetheless, as we cannot use a more sophisticated approach to correct for the clearly important effect of shock motion we take this approach in the remainder of this section. The results presented are similar, and conclusions drawn the same, if we only consider the crossings associated with a clear foot feature and make the correction based on the foot-estimated speeds (see Figure 5c).

[35] Figure 6 presents an examination of the dependence of the electron heating on different parameters, using the results presented in Figure 5d. The number of days between the time of a crossing and the nearest time of apparent opposition does not appear to affect the measured shock electron heating, and neither does θ_{Bn} (see Figures 6a and 6b). Owing to the lack of upstream ion parameters (see section 2) we have not been able to consider the effect of the upstream plasma β (total plasma pressure divided by magnetic pressure), another important shock parameter. We note that *Schwartz et al.* [1988] found no significant correlation between this quantity and the extent of electron heating.

[36] However, M_A* does have a clear influence on the extent of electron heating at the shock. Figure 6c shows that although the greater the normal proton kinetic energy the greater the electron heating at the shock, the highest Mach numbers were associated with the lowest electron temperature differences at their respective incident energies. Although the upper limit of the color scale in Figure 6c is 40, the highest Mach number crossings correspond to values above this.

[37] To investigate this Mach number effect further we normalized ΔT_e to the incident proton kinetic energy. Figure 7a shows a histogram of this normalized ΔT_e, which gives the fraction of the incident energy that is transferred into electron thermal energy at the shock. This fraction is generally between 3% and 7%. Figure 7b shows how the normalized electron temperature difference varies with M_A*, examining the effect that is apparent in Figure 6c in more detail. Despite the relatively large uncertainties, it is still clear that the higher the Mach number the lower the fraction of the incident kinetic energy that is transferred to the electrons as thermal energy.

[38] The rough separation of the inbound and outbound crossing data points by normalized ΔT_e is a by-product of our crude correction for shock motion (see Figure 7b). As discussed earlier in this section the correction leads to a clear separation between inbound and outbound crossings by incident ion kinetic energy, despite the significant overlap in the extent of electron heating (see Figure 5d). This explains the greater values of normalized ΔT_e for the outbound crossings than for the inbound crossings; thus there is no evidence that this is a real effect. We note that the Mach number effect on normalized ΔT_e is also clear when only the inbound or only the outbound crossings are considered, suggesting that our identification of this effect is not sensitive to our approach to correcting for shock motion. The main source of the large uncertainties shown in Figure 7 is this correction, where we took an error of 100% in our assumed shock speeds in order to cover the full range of physically reasonable values (see section 3).

[39] These results are in agreement with the findings of *Schwartz et al.* [1988] who analyzed a number of spacecraft crossings of collisionless shocks and also found that stronger shocks are less efficient electron heaters (see discussion in section 1). However, the study carried out by these authors only applied to Alfvén Mach numbers up to ~28, with relatively few values above 10; whereas in this study 52% of the Alfvén Mach numbers are above 10, and the highest value is ~150. The highest of these values result from a combination of atypically low upstream magnetic field strength and atypically high upstream electron number density, leading to the lowest upstream Alfvén speeds.

[40] We note that microinstabilities that grow in the foot region of some high–Mach number shocks have been predicted to produce strong electron heating [e.g., *Matsukiyo*

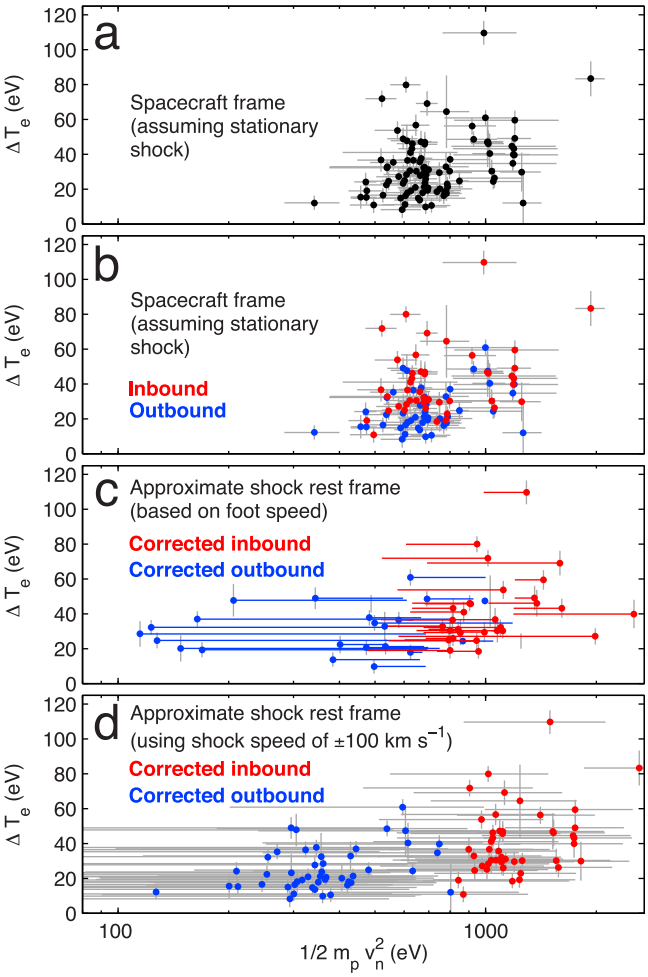

Figure 5. Plots of electron temperature difference across Saturn's bow shock ΔT_e against incident proton kinetic energy in the shock normal direction 1/2 m_p v_n^2. (a) Assuming stationary shock. (b) Assuming stationary shock, with the direction of each crossing indicated. (c) Using the approximate shock rest frame only for crossings where the shock speed was determined on the basis of a shock foot signature. Horizontal lines show the extent of the correction to the case where a stationary shock is assumed. (d) Using the approximate shock rest frame based on the assumption of a shock speed in the normal direction of +100 ± 100 km s^{-1} for all inbound crossings and −100 ± 100 km s^{-1} for all outbound crossings, where positive values are away from the planet and negative values are toward the planet.

and Scholer, 2006]. However, our results do not reveal clear evidence for this additional electron heating at the highest Mach numbers. The lack of evidence for foot microinstability-driven heating may be due to the restricted region of parameter space covered by our data set.

[41] The cross-shock potential in the H-T frame $\Delta\varphi^{HT}$ is related to the change in the electron temperature across the shock by

$$e\Delta\phi^{HT} \approx \frac{\gamma}{\gamma - 1}\Delta T_e, \qquad (5)$$

where e is the elementary charge and γ is the adiabatic index [e.g., *Schwartz et al.*, 1988]. In our analysis we have used ΔT_e rather than $e\Delta\varphi^{HT}$ because we are unable to measure the value of γ appropriate for Saturn's bow shock. However, assuming that γ = 5/3 (corresponding to a monatomic gas with 3 degrees of freedom) and using the mean value of ΔT_e from our data set (33.1 eV) allows us to determine a typical value of $\Delta\varphi^{HT}$ for Saturn's bow shock of ~80 V.

5. Summary

[42] In this paper we have analyzed data taken by the Cassini spacecraft during crossings of Saturn's bow shock. We have performed the first investigation of electron heating at Saturn's bow shock, combining Cassini observations of plasma parameters upstream and downstream of the shock with the results of a solar wind simulation. We found a positive correlation between the difference in the electron temperature across the shock and the incident flow kinetic energy, in agreement with current understanding of the nature of electron heating at collisionless shocks. Our results confirm

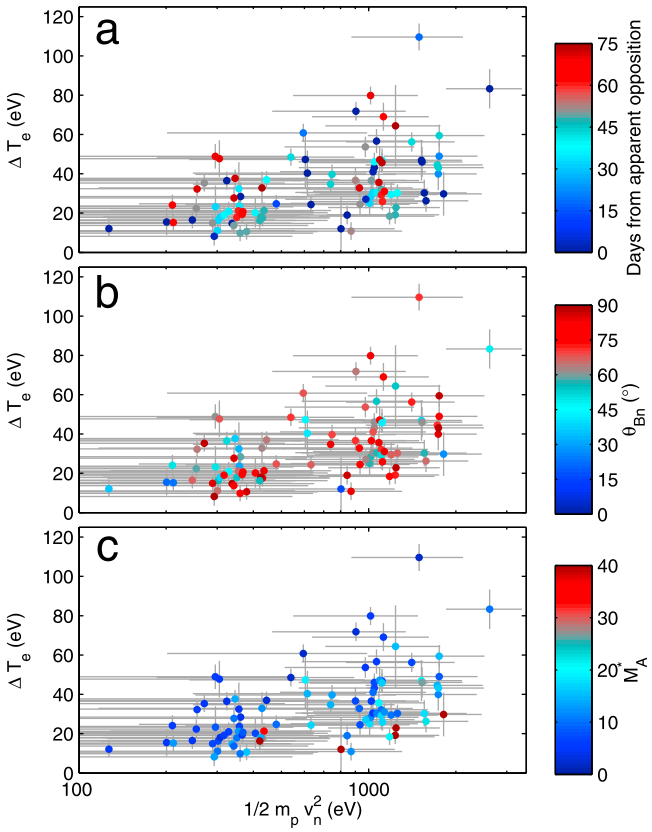

Figure 6. Plots of electron temperature difference across Saturn's bow shock ΔT_e against incident proton kinetic energy in the shock normal direction 1/2 m_p v_n^2 that include an examination of the influence of different parameters. All figures are based on the data presented in Figure 5d. (a) Color of data points indicates associated time from the nearest time of apparent opposition. (b) Color of data points indicates associated shock angle θ_{Bn}. (c) Color of data points indicates associated Alfvén Mach number M_A* (see Figure 3f).

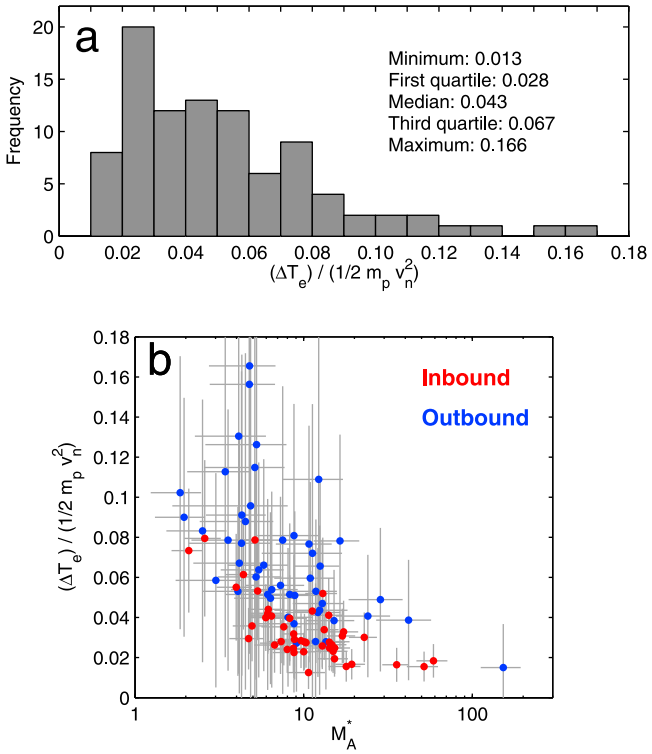

Figure 7. Normalized electron temperature difference at Saturn's bow shock and Mach number dependence. All figures are based on the data presented in Figure 5d. (a) Histogram of electron temperature difference normalized to the incident proton kinetic energy in the shock normal direction $\Delta T_e/1/2\ m_p\ v_n^2$. (b) Normalized electron temperature difference against Alfvén Mach number M_A* (see Figure 3f). The direction of each crossing is indicated. Note that the separation of inbound and outbound crossing data points is a by-product of our imperfect correction for shock motion and should not be interpreted as a real effect (see section 4).

the Mach number dependence of the extent of electron heating, where the fraction of the energy dissipated at the shock that is transferred to electron thermal energy decreases as the Mach number increases. We have derived Alfvén Mach numbers that are higher than those used in previous studies to assess this effect, the highest of which is ~150.

[43] The set of shock properties and assessment of electron heating presented here could form the basis of future, more detailed, studies of Saturn's bow shock. This shock wave is of particular interest because it is one of the strongest shocks ever observed by spacecraft (as revealed by the Mach numbers calculated in this study), and because the number of Cassini crossings of the boundary makes statistical studies possible. A specific topic of interest is particle acceleration at high–Mach number shocks [e.g., *Shimada and Hoshino*, 2000], since it has been proposed that this shock-related acceleration is responsible for cosmic rays [*Drury*, 1995; *Aharonian et al.*, 2004; *Uchiyama et al.*, 2007]. A further examination of the strongest shocks identified in this study, with an emphasis on extracting information from Cassini ion and energetic particle data, would be an important step toward understanding more about the physics of shocks in more extreme astrophysical environments.

[44] **Acknowledgments.** We acknowledge the support of the MAG and CAPS data processing and distribution staff and L. K. Gilbert and G. R. Lewis for ELS data processing. This work was supported by UK STFC through rolling grants to MSSL/UCL and Imperial College London.
[45] Masaki Fujimoto thanks the reviewers for their assistance in evaluating this manuscript.

References

Achilleos, N., et al. (2006), Orientation, location and velocity of Saturn's bow shock: Initial results from the Cassini spacecraft, *J. Geophys. Res.*, *111*, A03201, doi:10.1029/2005JA011297.
Aharonian, F. A., et al. (2004), High-energy particle acceleration in the shell of a supernova remnant, *Nature*, *432*, 75–77, doi:10.1038/nature02960.
Bale, S. D., et al. (2005), Quasi-perpendicular shock structure and processes, *Space Sci. Rev.*, *118*, 161–203, doi:10.1007/s11214-005-3827-0.
Burgess, D. (1995), Collisionless shocks, in *Introduction to Space Physics*, edited by M. G. Kivelson and C. T. Russell, pp. 129–163, Cambridge Univ. Press, New York.
Burgess, D., et al. (2005), Quasi-parallel shock structure and processes, *Space Sci. Rev.*, *118*, 205–222, doi:10.1007/s11214-005-3832-3.
Dougherty, M. K., et al. (2004), The Cassini magnetic field investigation, *Space Sci. Rev.*, *114*, 331, doi:10.1007/s11214-004-1432-2.
Drury, L. O. (1995), Particle acceleration in shocks, *Astrophys. Space Sci.*, *233*, 251–260, doi:10.1007/BF00627356.
Eastwood, J. P., et al. (2005), The foreshock, *Space Sci. Rev.*, *118*, 41–94, doi:10.1007/s11214-005-3824-3.
Fairfield, D. H. (1976), A summary of observations of the Earth's bow shock, in *Physics of Solar Planetary Environments: Proceedings of the International Symposium on Solar-Terrestrial Physics, June 7–18 1976, Boulder, Colorado*, vol. 2, edited by D. J. Williams, pp. 511–525, AGU, Washington, D. C.
Feldman, W. C., S. J. Bame, S. P. Gary, J. T. Gosling, D. McComas, M. F. Thomsen, G. Paschmann, N. Sckopke, M. M. Hoppe, and C. T. Russell (1982), Electron heating within the Earth's bow shock, *Phys. Rev. Lett.*, *49*, 199–201, doi:10.1103/PhysRevLett.49.199.
Formisano, V. (1982), Measurement of the potential drop across the Earth's collisionless bow shock, *Geophys. Res. Lett.*, *9*, 1033–1036, doi:10.1029/GL009i009p01033.
Gedalin, M. (1997), Ion dynamics and distribution at the quasi-perpendicular collisionless shock front, *Surv. Geophys.*, *18*, 541–566, doi:10.1023/A:1006509702173.
Goodrich, C. C., and J. D. Scudder (1984), The adiabatic energy change of plasma electrons and the frame dependence of the cross-shock potential at collisionless magnetosonic shock waves, *J. Geophys. Res.*, *89*, 654–6662.
Gosling, J. T., and A. E. Robson (1985), Ion reflection, gyration, and dissipation at supercritical shocks, in *Collisionless Shocks in the Heliosphere: Reviews of Current Research*, *Geophys. Monogr. Ser.*, vol. 35, edited by B. T. Tsurutani and R. G. Stone, pp. 141–152, AGU, Washington, D. C.
Gosling, J. T., and M. F. Thomsen (1985), Specularly reflected ions, shock foot thicknesses, and shock velocity determinations in space, *J. Geophys. Res.*, *90*, 9893–9896, doi:10.1029/JA090iA10p09893.
Horbury, T. S., P. J. Cargill, E. A. Lucek, J. Eastwood, A. Balogh, M. W. Dunlop, K.-H. Fornacon, and E. Georgescu (2002), Four spacecraft measurements of the quasiperpendicular terrestrial bow shock: Orientation and motion, *J. Geophys. Res.*, *107*(A8), 1208, doi:10.1029/2001JA000273.
Hull, A. J., J. D. Scudder, R. J. Fitzenreiter, K. W. Ogilvie, J. A. Newbury, and C. T. Russell (2000), Electron temperature and de Hoffmann–Teller potential change across the Earth's bow shock: New results from ISEE 1, *J. Geophys. Res.*, *105*, 20,957–20,971, doi:10.1029/2000JA900049.
Jackman, C. M., N. Achilleos, E. J. Bunce, S. W. H. Cowley, M. K. Dougherty, G. H. Jones, S. E. Milan, and E. J. Smith (2004), Interplanetary magnetic field at ~9 AU during the declining phase of the solar cycle and its implications for Saturn's magnetospheric dynamics, *J. Geophys. Res.*, *109*, A11203, doi:10.1029/2004JA010614.
Jackman, C. M., R. J. Forsyth, and M. K. Dougherty (2008), The overall configuration of the interplanetary magnetic field upstream of Saturn as revealed by Cassini observations, *J. Geophys. Res.*, *113*, A08114, doi:10.1029/2008JA013083.
Kanani, S. J., et al. (2010), A new form of Saturn's magnetopause using a dynamic pressure balance model, based on in situ, multi-instrument

Cassini measurements, *J. Geophys. Res.*, *115*, A06207, doi:10.1029/2009JA014262.

Kennel, C. F., J. P. Edmiston, and T. Hada (1985), A quarter century of collisionless shock research, in *Collisionless Shocks in the Heliosphere: A Tutorial Review*, *Geophys. Monogr. Ser.*, vol. 34, edited by R. G. Stone and B. T. Tsurutani, pp. 1–36, AGU, Washington, D. C.

Lewis, G. R., et al. (2008), Derivation of density and temperature from the Cassini-Huygens CAPS electron spectrometer, *Planet. Space Sci.*, *56*, 901–912, doi:10.1016/j.pss.2007.12.017.

Masters, A., C. S. Arridge, M. K. Dougherty, C. Bertucci, L. Billingham, S. J. Schwartz, C. M. Jackman, Z. Bebesi, A. J. Coates, and M. F. Thomsen (2008), Cassini encounters with hot flow anomaly-like phenomena at Saturn's bow shock, *Geophys. Res. Lett.*, *35*, L02202, doi:10.1029/2007GL032371.

Masters, A., et al. (2009), Hot flow anomalies at Saturn's bow shock, *J. Geophys. Res.*, *114*, A08217, doi:10.1029/2009JA014112.

Matsukiyo, S., and M. Scholer (2006), On microinstabilities in the foot of high Mach number perpendicular shocks, *J. Geophys. Res.*, *111*, A06104, doi:10.1029/2005JA011409.

Peredo, M., J. Slavin, E. Mazur, and S. Curtis (1995), Three-dimensional position and shape of the bow shock and their variation with Alfvénic, sonic and magnetosonic Mach numbers and interplanetary magnetic field orientation, *J. Geophys. Res.*, *100*, 7907–7916, doi:10.1029/94JA02545.

Russell, C. T. (1985), Planetary bow shocks, in *Collisionless Shocks in the Heliosphere: Reviews of Current Research*, *Geophys. Monogr. Ser*, vol. 35, edited by B. T. Tsurutani and R. G. Stone, pp. 109–130, AGU, Washington, D. C.

Russell, C. T., et al. (1982), Overshoots in planetary bow shocks, *Nature*, *296*, 45–48, doi:10.1038/296045a0.

Schwartz, S. J., M. Thomsen, and J. Gosling (1983), Ions upstream of the Earth's bow shock: A theoretical comparison of alternative source populations, *J. Geophys. Res.*, *88*, 2039–2047, doi:10.1029/JA088iA03p02039.

Schwartz, S. J., M. F. Thomsen, S. J. Bame, and J. Stansberry (1988), Electron heating and the potential jump across fast mode shocks, *J. Geophys. Res.*, *93*, 12,923–12,931, doi:10.1029/JA093iA11p12923.

Sckopke, N., G. Paschmann, S. J. Bame, J. T. Gosling, and C. T. Russell (1983), Evolution of ion distributions across the nearly perpendicular bow shock: Specularly and non-specularly reflected gyrating ions, *J. Geophys. Res.*, *88*, 6121–6136, doi:10.1029/JA088iA08p06121.

Scudder, J. D. (1995), A review of the physics of electron heating at collisionless shocks, *Adv. Space Res.*, *15*, 181–223, doi:10.1016/0273-1177(94)00101-6.

Shimada, N., and M. Hoshino (2000), Strong electron acceleration at high Mach number shock waves: Simulation study of electron dynamics, *Astrophys. J.*, *543*, L67–L71, doi:10.1086/318161.

Slavin, J. A., E. J. Smith, J. R. Spreiter, and S. S. Stahara (1985), Solar wind flow about the outer planets: Gas dynamic modeling of the Jupiter and Saturn bow shocks, *J. Geophys. Res.*, *90*, 6275–6286, doi:10.1029/JA090iA07p06275.

Smith, E. J. (1985), Interplanetary shock phenomena beyond 1 AU, in *Collisionless Shocks in the Heliosphere: Reviews of Current Research*, *Geophys. Monogr. Ser.*, vol. 35, edited by B. T. Tsurutani and R. G. Stone, pp. 69–83, AGU, Washington, D. C.

Thomsen, M. F., M. M. Mellott, J. A. Stansberry, S. J. Bame, J. T. Gosling, and C. T. Russell (1987), Strong electron heating at Earth's bow shock, *J. Geophys. Res.*, *92*, 10,119–10,124, doi:10.1029/JA092iA09p10119.

Thomsen, M. F., D. B. Reisenfeld, D. M. Delapp, R. L. Tokar, D. T. Young, F. J. Crary, E. C. Sittler, M. A. McGraw, and J. D. Williams (2010), Survey of ion plasma parameters in Saturn's magnetosphere, *J. Geophys. Res.*, *115*, A10220, doi:10.1029/2010JA015267.

Uchiyama, Y., F. A. Aharonian, T. Tanaka, T. Takahashi, and Y. Maeda (2007), Extremely fast acceleration of cosmic rays in a supernova remnant, *Nature*, *449*, 576–578, doi:10.1038/nature06210.

Went, D. R., G. B. Hospodarsky, A. Masters, K. C. Hansen, and M. K. Dougherty (2011), A new semi-empirical model of Saturn's bow shock based on propagated solar wind parameters, *J. Geophys. Res.*, *116*, A07202, doi:10.1029/2010JA016349.

Woods, L. C. (1971), On double-structured, perpendicular, magnetoplasma shock waves, *Plasma Phys.*, *13*, 289–302, doi:10.1088/0032-1028/13/4/302.

Young, D. T., et al. (2004), Cassini plasma spectrometer investigation, *Space Sci. Rev.*, *114*, 1–112, doi:10.1007/s11214-004-1406-4.

Zieger, B., and K. C. Hansen (2008), Statistical validation of a solar wind propagation model from 1 to 10 AU, *J. Geophys. Res.*, *113*, A08107, doi:10.1029/2008JA013046.

N. Achilleos, Centre for Planetary Sciences, University College London–Birkbeck, Gower Street, London WC1E 6BT, UK.

A. J. Coates and A. Masters, Mullard Space Science Laboratory, Department of Space and Climate Physics, University College London, Holmbury Street Mary, Dorking, Surrey RH5 6NT, UK. (am2@mssl.ucl.ac.uk)

M. K. Dougherty, E. M. Henley, J. Mitchell, and S. J. Schwartz, Space and Atmospheric Physics Group, Blackett Laboratory, Imperial College London, Prince Consort Road, London SW7 2AZ, UK.

K. C. Hansen, Department of Atmospheric, Oceanic, and Space Sciences, University of Michigan, 2455 Hayward St., Ann Arbor, MI 48109, USA.

M. F. Thomsen, Space Science and Applications, Los Alamos National Laboratory, Los Alamos, NM 87545, USA.

B. Zieger, Space Research Institute, Austrian Academy of Sciences, Schmiedlstr. 6, A-8042 Graz, Austria.